Optics Letters

Using temperature to reduce noise in quantum frequency conversion

Paulina S. Kuo,[1,*] Jason S. Pelc,[2] Carsten Langrock,[2] and M. M. Fejer[2]

[1]Information Technology Laboratory, National Institute of Standards and Technology, 100 Bureau Drive, Gaithersburg, Maryland 20899, USA
[2]E. L. Ginzton Laboratory, Stanford University, 348 Via Pueblo Mall, Stanford, California 94305, USA
*Corresponding author: paulina.kuo@nist.gov

Received 14 February 2018; accepted 22 March 2018; posted 27 March 2018 (Doc. ID 320258); published 23 April 2018

Quantum frequency conversion is important in quantum networks to interface nodes operating at different wavelengths and to enable long-distance quantum communication using telecommunications wavelengths. Unfortunately, frequency conversion in actual devices is not a noise-free process. One main source of noise is spontaneous Raman scattering, which can be reduced by lowering the device operating temperature. We explore frequency conversion of 1554 nm photons to 837 nm using a 1813 nm pump in a periodically poled lithium niobate waveguide device. By reducing the temperature from 85°C to 40°C, we show a three-fold reduction in dark count rates, which is in good agreement with theory.

OCIS codes: (190.7220) Upconversion; (190.5650) Raman effect; (190.4360) Nonlinear optics, devices.

https://doi.org/10.1364/OL.43.002034

Future quantum networks will employ quantum frequency conversion (QFC) to connect nodes that operate at different wavelengths and to enable long-distance qubit transport at telecommunications wavelengths. QFC devices often consist of $\chi^{(2)}$ nonlinear waveguides, such as periodically poled lithium niobate (PPLN) waveguides [1–7]. Four-wave-mixing Bragg scattering using $\chi^{(3)}$ nonlinearities in waveguides and fibers [8–12] and in microresonators [13] has also been used for QFC. In ideal QFC, the wavelength of a photonic quantum state is converted to another wavelength with 100% efficiency while maintaining the quantum information [14]. In practice, system conversion efficiencies up to 86% in a single-stage [2] and 87% in a two-stage process [3] have been demonstrated.

Frequency conversion in practical devices is not a noise-free process. If we focus on $\chi^{(2)}$ devices, the main noise sources in such devices are spontaneous Raman scattering (SRS) and spontaneous parametric downconversion (SPDC) [2,15,16]. The strong, classical pump beam drives spontaneous, inelastic scattering processes, which generate photons that may overlap in wavelength with the signal photons or the target photons. These two mechanisms are illustrated in Fig. 1. Both of these spontaneous processes can be mitigated by choosing the pump to be the longest of the three interacting wavelengths in the QFC process [1,2]. The noise can be further reduced by increasing the spectral separation between the pump and the signal [2,17]. When the pump is the longest wavelength, SPDC does not produce photons at the signal or target wavelengths, but anti-Stokes Raman scattering may still contribute (see Fig. 1). It was previously shown that narrowband filtering can reduce noise, since the noise processes are generally broadband, while the signal photons are narrowband [16]. The noise can also be reduced by lowering the operating temperature of the QFC device due to the temperature-dependent nature of Raman scattering. In this Letter, we describe the theoretically expected anti-Stokes Raman scattering noise, and we show that predicted temperature-dependent noise count rates agree well with experimental measurements. These results confirm that anti-Stokes Raman scattering is the dominant noise process in long-wavelength-pumped PPLN waveguide QFC devices.

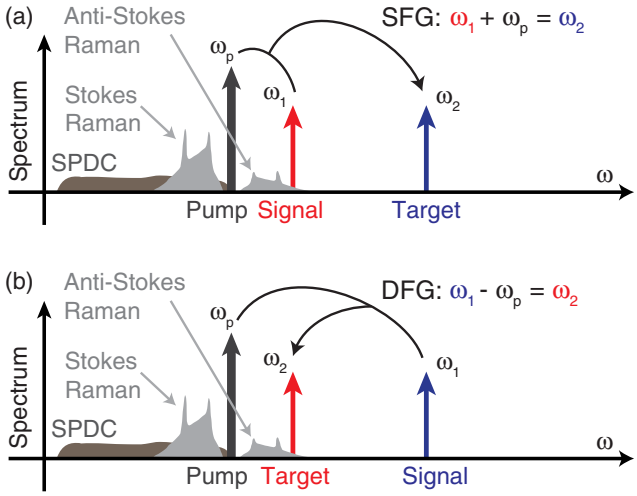

Fig. 1. Illustration of noise processes for (a) sum- and (b) difference-frequency generation (SFG and DFG, respectively). In both cases, the pump is the longest wavelength (lowest frequency). In (a), spontaneous anti-Stokes Raman scattering overlaps with the signal, and both signal and noise get upconverted to the target. In (b), anti-Stokes Raman scattered photons are generated directly at the target wavelength.

The anti-Stokes Raman scattering intensity is described by [2,18]

$$I(\Delta\nu, T) = I_0\sigma(\Delta\nu)n(\Delta\nu, T), \quad (1)$$

where

$$n(\Delta\nu, T) = \left[\exp\left(\frac{hc|\Delta\nu|}{kT}\right) - 1\right]^{-1}, \quad (2)$$

is the phonon occupation number, h is Planck's constant, $\Delta\nu$ is the frequency detuning (in cm^{-1}) between the Raman-scattered photon and the pump (which is negative for an anti-Stokes Raman scattered photon), c is the speed of light (in cm/s), k is the Boltzmann constant, and T is the temperature. I_0 is a reference anti-Stokes Raman scattering intensity that depends on the collection efficiency of the Raman scattered photons and is independent of temperature and photon frequencies. The frequency-dependent cross section, $\sigma(\Delta\nu)$, describes the Raman spectrum. Over the temperature range explored here, the Raman spectrum of lithium niobate (LN) is essentially independent of temperature, but care must be taken over larger temperature ranges [19]. The Raman spectrum for LN is presented in Ref. [2] and shows two major peaks at $\Delta\nu = -260$ cm^{-1} and -630 cm^{-1}.

To measure the temperature dependence of the generated noise, we performed frequency conversion in a PPLN waveguide (see Fig. 2 for the experimental setup). We used a 18.9 μm period, 52 mm long, reverse-proton-exchanged PPLN waveguide. The waveguide device was designed for upconversion detection of C-band photons; more specifically, it was designed for sum-frequency generation (SFG) between an 1813 nm pump and a 1554 nm signal at 40°C, with a corresponding SFG wavelength of 837 nm. The input to the waveguide was fiber-pigtailed. The pump consisted of an external-cavity diode laser followed by a thulium-doped fiber amplifier (TDFA) that produced up to 400 mW of power. After the TDFA, we inserted four 1550 nm/1800 nm wavelength division multiplexers to reject any amplified spontaneous emission at the signal wavelength. While holding the pump wavelength fixed, we varied the PPLN waveguide temperature between 40°C and 85°C, which caused the phasematched signal wavelength to tune between 1554 nm and 1566 nm (and the corresponding SFG wavelength to tune from 837 nm to 840 nm). The upconverted photons were filtered and detected with a Si avalanche photodiode (APD, PerkinElmer SPCM-AQR-14). A pair of prisms arranged near Brewster's angle was placed after the waveguide and used to separate residual pump and signal beams from the upconverted photons. We also used a volume Bragg grating (VBG, Optigrate) tunable between 835 nm and 840 nm to reduce the optical detection bandwidth and thus reduce the Raman noise counts. At near-normal incidence, the VBG bandwidth (0.05 nm full width at half-maximum) is independent of the center wavelength but the diffraction efficiency slightly decreases as the angle of incidence increases (tuning towards shorter wavelength). In the analysis, we accounted for the wavelength-dependent reflection of the VBG by dividing the dark count rates (DCRs) by the system detection efficiency.

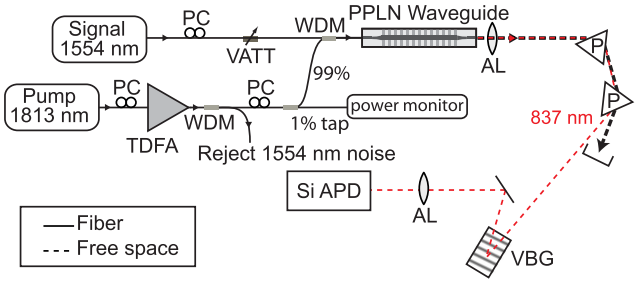

Fig. 2. Experimental setup. PC, polarization controller; VATT, variable attenuator; WDM, wavelength division multiplexer; AL, aspheric lens; P, prism; TDFA, thulium-doped fiber amplifier; Si APD, silicon avalanche photodiode; VBG, volume Bragg grating.

Figure 3 plots experimental measurements of DCRs, total APD count rates, and system detection efficiencies as a function of incident pump power for several different PPLN temperatures. We recorded the total count rate of the APD with the signal blocked and unblocked, with the former measurement giving the DCR. The DCR measured by the APD is the sum of detector dark counts and Raman noise counts. From our measurements, we estimate the APD detector DCR to be about 300 counts per second (s^{-1}). The system detection efficiency, $\eta(P)$, was calculated by subtracting the dark count rate from the total count rate and then dividing by the photon flux at the input fiber. This efficiency includes losses and the detection efficiency of the APD, which for wavelengths around 840 nm, is between 50% and 55% [20]. The system detection efficiency data were fitted to [1]

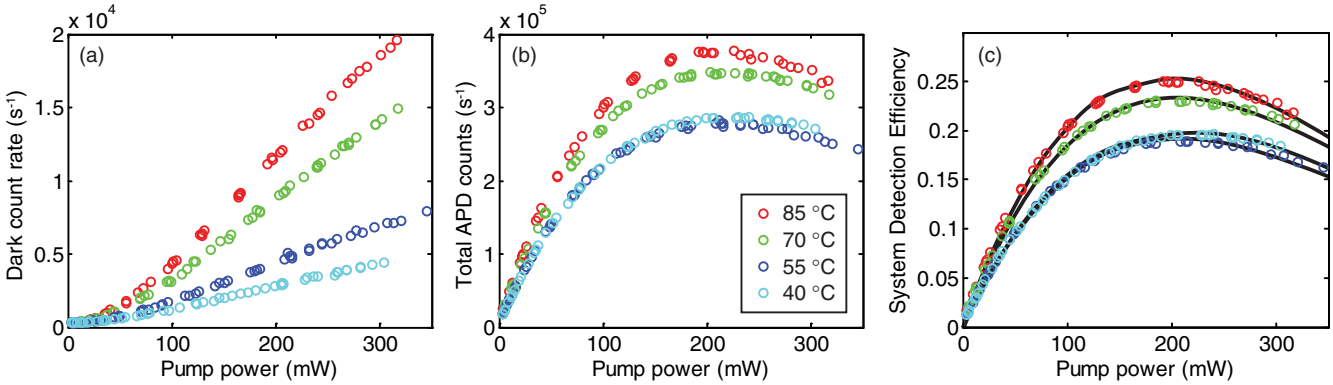

Fig. 3. Measured (a) dark count rates, (b) total APD count rates, and (c) system conversion efficiencies at different PPLN temperatures. Black lines are fits to Eq. (3).

Table 1. Frequency Conversion Temperature Tuning Results[a]

Temperature (°C)	Signal Wavelength (nm)	$\Delta\nu$ (cm^{-1})	P_{max} (mW)[b]	$\eta(P_{max})$[c]	DCR(P_{max}) (s^{-1})[d]
40	1554.14	−917.3	215.4	0.20	2.79×10^3
55	1557.49	−903.5	207.8	0.19	4.38×10^3
70	1561.41	−887.4	204.5	0.23	8.74×10^3
85	1565.57	−870.4	199.9	0.25	11.4×10^3

[a]Pump wavelength was fixed at 1812.55 nm.
[b]Pump power at maximum conversion.
[c]Maximum system conversion efficiency.
[d]Dark count rate at maximum conversion.

$$\eta(P) = \eta_0 \sin^2\left(\sqrt{\eta_{nor} P} L\right), \tag{3}$$

where η_{nor} is the normalized nonlinear conversion efficiency in the low-conversion limit, and L is the length of the PPLN grating. η_0 is the maximum efficiency, which includes the APD efficiency, fiber coupling losses, and imperfect photon collection. P_{max}, the pump power at maximum conversion, is related to the other parameters by

$$P_{max} = \pi^2/(4\eta_{nor} L^2). \tag{4}$$

The data in Fig. 3(a) show that with the VBG, the DCRs were as high as 2×10^4 s^{-1}. We chose the signal photon flux to be sufficiently large, such that the count rate due to converted signal photons was much larger than the noise count rate, while also keeping the total APD count rate below 10^6 s^{-1} where the APD count rate is linear in intensity [20]. The narrowband VBG was critical for reducing the noise counts in order to achieve these conditions. In our experiment, the incident signal flux before the PPLN device was set to 1.45×10^6 s^{-1}, which resulted in total APD count rates that did not exceed 4×10^5 s^{-1}.

Table 1 presents the measured efficiencies and DCRs for different device temperatures. The table lists the detuning between the signal and pump ($\Delta\nu$), as well as the pump power of maximum conversion (P_{max}), the maximum system detection efficiency ($\eta(P_{max})$), and the DCR at maximum conversion (DCR(P_{max})). P_{max} was calculated from Eq. (4) using parameters determined by fitting the data to Eq. (3). Variations in collection efficiency due to the VBG and non-ideal photon collection can be seen in the non-monotonic nature of measurements of $\eta(P_{max})$.

Data from Table 1 are plotted in Fig. 4 and compared to theory. Figure 4(a) shows the Raman cross section near $\Delta\nu = -900$ cm^{-1} normalized to the peak value near $\Delta\nu = -880$ cm^{-1}. Red dots are spontaneous Raman spectrum measurements taken with a Raman microscope (see Ref. [2] for details). The solid curve is a polynomial fit to the data over this range; this fit was used for subsequent calculations of expected SRS noise using Eqs. (1) and (2) [solid curve in Fig. 4(b)]. Figure 4(b) shows the corrected noise counts, DCR(P_{max})/$\eta(P_{max})$, normalized to the value at $T = 40$°C. As mentioned earlier, the correction was needed to account for imperfect photon collection. The theoretical prediction (solid line) and experimental data (open circles) show very good agreement. For our device, we observed a three-fold decrease in corrected noise count rates when the PPLN temperature was reduced from 85°C to 40°C.

Temperature affects noise from SRS through two effects: the phonon occupation number, $n(\Delta\nu, T)$, and shifts in $\Delta\nu$ due to tuning of the phasematching wavelength, which affects both $n(\Delta\nu, T)$ and $\sigma(\Delta\nu)$. For LN, the Raman spectrum for detunings $|\Delta\nu| > 1000$ cm^{-1} is fairly flat, making the $n(\Delta\nu, T)$ term more important in this range. For $|\Delta\nu| < 800$ cm^{-1}, the Raman spectrum exhibits significant structure due to the two peaks at $\Delta\nu = -260$ cm^{-1} and -630 cm^{-1} (see Ref. [2]). In this detuning range, changing temperature affects SRS predominantly through $\sigma(\Delta\nu)$. Our particular frequency-conversion

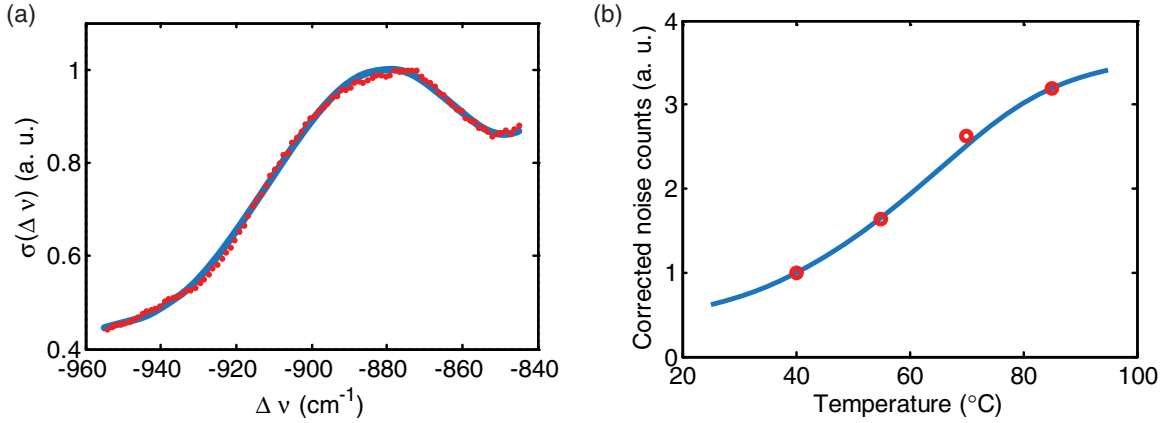

Fig. 4. (a) Normalized Raman cross-section for PPLN near -900 cm^{-1} detuning. The red dots are spontaneous Raman scattering spectral measurements, and the solid line is a polynomial fit. (b) Corrected noise counts normalized to value at $T = 40$°C. Open circles are experimental measurements, and the solid line is predicted noise due to anti-Stokes Raman scattering [Eqs. (1) and (2)].

device was designed for detunings in the vicinity of $|\Delta\nu| \approx 900\ \mathrm{cm}^{-1}$ where both $n(\Delta\nu, T)$ and $\sigma(\Delta\nu)$ terms are significant. Ignoring changes in the cross section $\sigma(\Delta\nu)$, only a two-fold decrease in noise would have been expected in our device from the phonon occupation number.

This work suggests a promising path forward for reducing noise counts in PPLN waveguides used in quantum frequency conversion. We note that the strategy of reducing temperature to reduce SRS noise has been successfully applied in fiber-based four-wave-mixing Bragg scattering for QFC [12], and in fiber-based photon-pair sources where the fibers are cooled to 77 K [21] and 4 K [22]. If we consider more modest cooling using a single-stage Peltier cooler that can achieve −40°C [23], we expect an 11-fold decrease in noise count rate compared to operating at 40°C. Taking the measured DCR at 40°C and assuming identical filtering and system detection efficiency, we would predict the noise count rate for our device at −40°C to be 250 s^{-1}, which is below our APD's detector DCR. Typical detector DCRs for superconducting nanowire single-photon detectors are around 10 s^{-1} [24]. By a similar calculation, we predict that we would need to operate our upconversion QFC device at −110°C to achieve a 10 s^{-1} noise count rate. When operating fiber-pigtailed PPLN devices at low temperatures, challenges may exist, such as possible photorefractive damage [25] or thermal expansion mismatch between the fiber pigtail and the PPLN crystal. Also, the poling period must be properly chosen for a desired set of QFC wavelengths in order to achieve phasematching at the specific operating temperature.

We have presented the temperature dependence of noise due to anti-Stokes Raman scattering. We show that temperature affects the noise through the phonon occupation number, and through changes in the phasematching wavelengths and therefore in the Raman cross section. For our PPLN waveguide over the temperature range we examined, both factors are important. We observed very good agreement between our measurements and theoretical predictions. The theory also predicts a significant drop in noise from SRS when the QFC device is operated at low temperatures; we expect an order of magnitude reduction in Raman noise counts at −40°C compared to 40°C and reduction in noise counts to negligible levels (less than 0.001 s^{-1}) at liquid nitrogen temperatures. This technique for reducing noise in quantum frequency conversion will be attractive in enabling high-fidelity quantum state translation for future hybrid quantum networks.

The identification of any commercial product or trade name does not imply endorsement or recommendation by the National Institute of Standards and Technology.

Funding. This work was partially supported by the Army Research Laboratory (ARL)'s Center for Distributed Quantum Information through the SciNet project.

REFERENCES

1. C. Langrock, E. Diamanti, R. V. Roussev, Y. Yamamoto, M. M. Fejer, and H. Takesue, Opt. Lett. **30**, 1725 (2005).
2. J. S. Pelc, L. Ma, C. R. Phillips, Q. Zhang, C. Langrock, O. Slattery, X. Tang, and M. M. Fejer, Opt. Express **19**, 21445 (2011).
3. J. S. Pelc, Q. Zhang, C. R. Phillips, L. Yu, Y. Yamamoto, and M. M. Fejer, Opt. Lett. **37**, 476 (2012).
4. J. S. Pelc, L. Yu, K. D. Greve, P. L. McMahon, C. M. Natarajan, V. Esfandyarpour, S. Maier, C. Schneider, M. Kamp, S. Höfling, R. H. Hadfield, A. Forchel, Y. Yamamoto, and M. M. Fejer, Opt. Express **20**, 27510 (2012).
5. S. Zaske, A. Lenhard, C. A. Kessler, J. Kettler, C. Hepp, C. Arend, R. Albrecht, W.-M. Schulz, M. Jetter, P. Michler, and C. Becher, Phys. Rev. Lett. **109**, 147404 (2012).
6. S. Ates, I. Agha, A. Gulinatti, I. Rech, M. T. Rakher, A. Badolato, and K. Srinivasan, Phys. Rev. Lett. **109**, 147405 (2012).
7. R. Ikuta, T. Kobayashi, S. Yasui, S. Miki, T. Yamashita, H. Terai, M. Fujiwara, T. Yamamoto, M. Koashi, M. Sasaki, Z. Wang, and N. Imoto, Opt. Express **22**, 11205 (2014).
8. H. J. McGuinness, M. G. Raymer, C. J. McKinstrie, and S. Radic, Phys. Rev. Lett. **105**, 093604 (2010).
9. I. Agha, S. Ates, M. Davanço, and K. Srinivasan, Opt. Express **21**, 21628 (2013).
10. P. S. Donvalkar, V. Venkataraman, S. Clemmen, K. Saha, and A. L. Gaeta, Opt. Lett. **39**, 1557 (2014).
11. B. A. Bell, J. He, C. Xiong, and B. J. Eggleton, Opt. Express **24**, 5235 (2016).
12. S. Clemmen, A. Farsi, S. Ramelow, and A. L. Gaeta, Phys. Rev. Lett. **117**, 223601 (2016).
13. Q. Li, M. Davanço, and K. Srinivasan, Nat. Photonics **10**, 406 (2016).
14. P. Kumar, Opt. Lett. **15**, 1476 (1990).
15. S. Zaske, A. Lenhard, and C. Becher, Opt. Express **19**, 12825 (2011).
16. P. S. Kuo, J. S. Pelc, O. Slattery, Y.-S. Kim, M. M. Fejer, and X. Tang, Opt. Lett. **38**, 1310 (2013).
17. Y.-H. Cheng, T. Thomay, G. S. Solomon, A. L. Migdall, and S. V. Polyakov, Opt. Express **23**, 18671 (2015).
18. R. H. Stolen, in *Optical Fiber Telecommunications*, S. E. Miller and A. G. Chynoweth, eds. (Academic, 1979), pp. 125–150.
19. W. D. Johnston and I. P. Kaminow, Phys. Rev. **168**, 1045 (1968).
20. "SPCM-AQRH single photon counting module," http://www.excelitas.com/Downloads/DTS_SPCM-AQRH.pdf.
21. H. Takesue and K. Inoue, Opt. Express **13**, 7832 (2005).
22. S. D. Dyer, M. J. Stevens, B. Baek, and S. W. Nam, Opt. Express **16**, 9966 (2008).
23. "TEC elements, resistive heaters, thermistors, and thermocouples," https://www.thorlabs.com/newgrouppage9.cfm?objectgroup_id=305.
24. M. D. Eisaman, J. Fan, A. Migdall, and S. V. Polyakov, Rev. Sci. Instrum. **82**, 071101 (2011).
25. C. Langrock, S. Kumar, J. E. McGeehan, A. E. Willner, and M. M. Fejer, J. Lightwave Technol. **24**, 2579 (2006).